Modeling of a Novel Vibrospring Particle-Size Distribution Analyzer

Haroun Mahgerefteh and Ali Shaeri
Dept. of Chemical Engineering, University College London, Torrington Place, London WC1E 7JE, U.K.

The design and modeling of a novel technique for particle-size distribution analysis are described. In its most basic form, the unit comprises a horizontally held closed-coil helical spring that is partly filled with the test powder and sinusoidally vibrated in the transverse direction. Particle-size distribution data are obtained by stretching the spring to known lengths and measuring the mass of the powder discharged from the spring resonant frequency. The spring's vibration characteristics, including the dynamic vibration profile as well as its first harmonic resonant frequency, are predicted using a viscoelastic model, which is in turn validated by comparison with experimental data. Particle-size distribution data are reported in conjunction with a variety of powders including glass Ballotini, grit stone, sand, and sawdust in the size range 30 − 800 μm. A typical reproducibility is ± 4%.

Introduction

Approximately 30% of the chemicals produced in the world are in the form of powder and nearly all aspects of the technology related to their manufacture, handling or application at some stage require a knowledge of the particle size (Allen, 1997). This statement encompasses a wide and diverse range of industries, including pharmaceuticals, energy production, ceramics, construction, paints, and foods. In the pharmaceuticals industry, for example, particle-size distribution affects important parameters such as bioavailability (the rate of uptake of drug in metabolism), dose uniformity (uniform mixing of the active ingredient within the binder), and formulation (such as controlled delivery of dosage, for example, in inhalers). In the cement industry, on the other hand, particle size has an important effect on both settling time and strength characteristics of concrete. Here, particle size also dictates the sintering rate as well as clinkering temperature of cement, both of which have a significant effect on fuel consumption (Muly and Frock, 1980).

In the energy sector, particle-size distribution of pulverized coal in steam power plants critically controls both the combustion efficiency as well as the amounts of the nitrous oxide pollutants generated during the combustion process.

In geology, particle sizing of sedimentary materials can give helpful information about their origin and history (Syvitski, 1991). Particle-size analysis has also huge applications in crystallization. In many industrial processes, the demand is for a narrow range of particle size, as regularity results in crystals having good storage and transportation properties as well as free-flowing characteristics (Mullin, 1993).

In fluidization, the minimum fluidization velocity of a bed subjected to an upward gas flow critically affects bed performance. This parameter is primarily dependent on the size of the particles making up the bed (Geldart, 1990; Yates et al., 1984; Wen and Yu, 1966).

The solubility of particles in liquids is governed by their size distribution. Interestingly, Gibbs-Thomson (Mullin, 1993) showed that solubility does not always improve with smaller particles. Numerous recent studies in air pollution (see, for example, Dockery et al., 1993; Pope et al., 1995; Walters et al., 1994) have indicated a direct relationship between particle size of airborne particulates and their harmful effects on the human respiratory system. Even the "sponginess" of cakes is dependent on the particle-size distribution of the flour used.

Such sustained and unrelenting demand for a knowledge of particle size has led to the development of a large number of particle-sizing techniques. According to a recent survey (Market Analysis and Perspective, Physical Property Measurements, 1993), worldwide sales of particle-sizing equipment in 1991−1992 exceeded $500 m. The same survey predicts that this figure is expected to grow by approximately

Correspondence concerning this article should be addressed to H. Mahgerefteh.

10% per annum. Allen (1997) cites over 50 methods for particle-size analysis based on a variety of principles with different degrees of sophistication.

Table 1 shows the relative merits and disadvantages as well as the principle of operation of some of the most widely used methods.

Typical drawbacks include cost, complicated use, the inability to handle relatively large samples (> 2 g), thus giving rise to representation problems, and the requirement for special sample preparation prior to analysis. Of these, despite their obvious disadvantages, sieves still remain by far the most widely used method of sizing powders. Ironically, the technology has changed relatively little despite more than 2000 years of development.

Another major problem associated with all the techniques cited is that none is capable of cost effectively sizing particles online. Although a recently developed laser diffraction technique involving the so-called "isokinetic" extraction of a representative test sample from the flowing particulate stream (by virtue of ensuring that there is no net change in velocity of the test sample from the process line) is claimed to be suitable for online operations, it is very expensive (ca. \$100,000), limited to sub-500 μm particles, and not suitable for use in hostile environments. Cost becomes a particularly acute problem during continuous process operations where multiple-point monitoring of particle-size distribution is often required.

For example, in the manufacture of industrial powders as diverse as paint pigments, ceramics, cement, and photocopier toner, it is necessary to tightly control the particle-size distribution. An online or rapid response capability allows immediate readjustment of the process parameters that control the particle size, if and when required. At present this either involves taking samples to the laboratory for analysis, often using sieves, and feeding the results to the process engineer sometime later. In some grinding operations, this problem is dealt with by excess grinding in order to ensure that the particle size falls within the required specification. In many instances, the preceding practice can lead to a considerable amount of wasted energy (grinding processes, for example, account for about 11% of the fuel consumption in cement manufacturing) as well as environmental problems associated with the disposal of "off-spec" products.

In this article we describe the basic design and modeling of a novel technique for particle-size analysis that overcomes most of the problems just cited. In its most basic form, the instrument comprises a horizontally held, close-coiled helical spring that is partly filled with the powder under test. The

Table 1. League Table of Most Commonly Used Particle Sizing Techniques

Technique	Principle	Size (μm)	Application	Test Time	Advantages	Disadvantages
Sieving Woven wire or Electroformed	Passing through apertures	> 35 5–100	Widely used in mineral processing	> 20 min	Simple, easy, cheap, covers a wide range of sizes, very common, no operator's skill is requires	Blinding and clearing problems. Sieves' wires easily get damaged and calibration problems occur
Microscopy Optical Electron	Scanning in a predetermined direction	1–150 0.01–5	General Airborne materials, crystals	Hours	Direct observation, examination of the shape, and morphology are possible	Labor-intensive, accuracy depends on operator's judgment, only 2-D. Unsuitable for routine analysis
Sedimentation Gravitational Centrifugal	Setting rate of particles in a fluid	1–75 0.075–5	Pharmaceutical powders, cement, metal powders	Slow A few min	Highly reproducible, widely used as a reference, inexpensive	Labor-intensive, particles must be dispersed well, unsuitable for a rapid settling rate, risk of fluid/particle interaction
Coulter counter (Allen 1977) Electrozone	Increase of electrical resistance of an electrolyte	0.6–250	First developed for counting blood cells, now used in industry	Rapid (20 s)	The only technique that measures equivalent volume diameter, wide size range, reproducible	Blockage of orifice, expensive, errors due to passage of bubbles through the orifice, risk of fluid/particle interaction
Laser diffraction	Light diffraction	0.3–1,500	Wide range of powders	Rapid (20 s)	Accurate, measures a variety of different characteristic sizes	Expensive, measured size may be affected by sample optical properties, small sample size, not robust

technique works on the basis of the simple fact that when the spring is stretched and vibrated in the transverse direction using simple harmonic motion, the particle size of the powder discharged from the spring coils is related to the spring extension. On the other hand, the weight of the powder discharged can be determined on a continuous basis by reference to the system's resonance characteristics. Data on the particle-size distribution are then provided as a simple plot of percentage mass of discharged powder vs. the corresponding particle size.

The development of a fully predictive mathematical model describing the vibration characteristics of the system is also described. Apart from predicting the variation of resonant frequency with sample mass, the model is used to generate the spring dynamic profile during oscillations. The latter information is shown to be important for an accurate prediction of the discharged particle size from a knowledge of the spring linear extension and the vibration intensity. The model can also serve as an important tool for design optimization purposes. Finally, the results of a series of tests establishing the capability of the system to produce particle-size distribution data for a variety of samples with different size, shape, and flow characteristics are presented.

Description of the apparatus

Figure 1 shows a basic design of the particle sizer. The unit comprises a horizontally held, closed-coil helical spring (1), one end of which is clamped to one side of the main chamber (2), while the other is permanently sealed and securely attached to a 100-mm-long M6×1.00 screw (3) via a positioning plate (4) mounted on two slide rails (5) and (6). The spring has squared ground ends, about 83 mm in length, 10 mm mean diameter, and is made from 0.92-mm steel wire. A feed elbow (7) made from a suitable material, such as a plastic, is used to direct the test powder into the spring via a 10-mm hole drilled into the side of the main chamber.

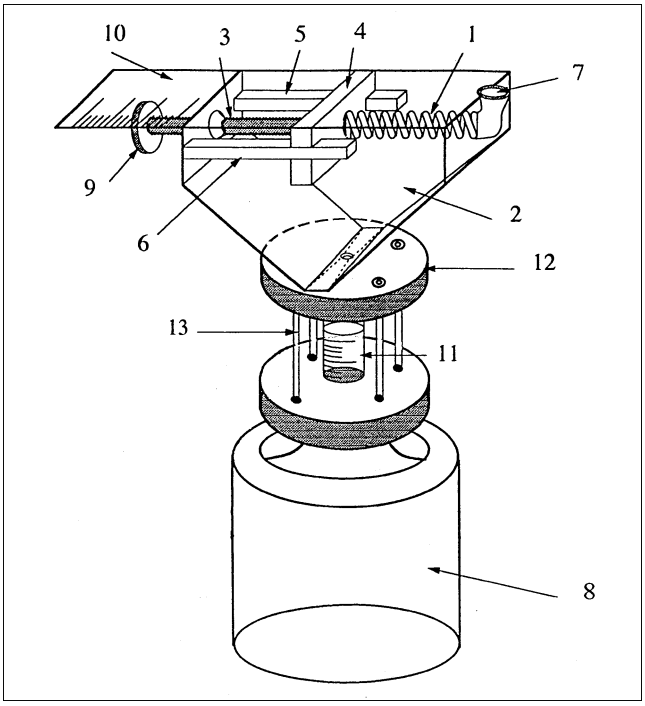

Figure 1. Vibrospring particle-size distribution analyzer.

The spring can be stretched by turning the screw (3), which is also threaded into the wall of the chamber (2). The extension of the spring, accompanied by its vibration at its first harmonic resonant frequency in the lateral direction using a standard electrodynamic vibration generator [(8), type V406, Link Dynamic Systems, 1988], results in the vibrofluidization and discharge of the test powder through the spring coils. The discharged particle size and the corresponding mass are in turn respectively determined from the spring extension and its resonant frequency. Particle-size distribution can be generated by repeating the same procedure at various spring extensions until complete discharge of the test powder. The spring lateral extension is measured by reference to the location of the extension screw head (9) in relation to the graduated scale (10). Resonant frequency and amplitude of vibration of the spring are measured using a phototransistor (RS type SF309FA) comprising a photodiode emitter and a photodiode detector mounted at a distance of about 1 cm above the midpoint of the spring.

The main chamber is suitably angled (45° to horizontal) in order to direct the discharged powder into the sample collector (11). A base disk (12) serves as the connection between the main chamber (2) and the sample collector (11). An alternative design (not shown) allows the collection of the separated fractions in a number of sample collectors mounted on a carousel. The base disk (12) also incorporates a tapered rectangular groove machined at its center that directs the discharged powder into the sample collector via a 10-mm-dia. threaded hole located at its center.

The whole assembly is mounted on top of the vibration generator (8) using four supporting rods (13) in the manner shown in the figure.

Electronic drive and detection systems

The system automatically tunes to the first harmonic resonant frequency of the spring by operating on the basis of a regenerative feedback loop (Mahgerefteh and Al-Khoory, 1991). In this case, the vibration-induced voltage signal picked up by the optical sensor is returned to drive the vibration generator via a 30-W pulsating alternating current power amplifier, thus forming a closed loop. The vibration generator comprises two armature drive coils of differing impedance. It has a rated peak sinusoidal force of 97.9 N, corresponding to maximum displacement and acceleration of 7 mm and 50 g, respectively. A 50-W transformer (RS type 223-8257) acts as the system power supply.

The optical sensors operate by illuminating the spring with an infrared light source of known wavelength in order to cast a shadow across the photodiodes, which in turn produce photocurrents proportional to the light intensity using a specially designed circuit (Mahgerefteh et al., 1994; Mahgerefteh and Khodaverdian, 1996). As the spring vibrates, the shadow oscillates across the surfaces of the photodiodes, thereby modulating the photocurrents. The difference between the photocurrents of the two detectors transformed into a voltage signal using an amplifier is linearly related (ca. 0.9980 correlation coefficient) to the spring displacement, provided the

shadow overlaps the two photodiodes. With this arrangement it is possible to detect amplitudes of vibration as low as 1×10^{-3} mm.

A variable band-pass filter (range 0–230 Hz) eliminates second- and higher-order harmonics. The amplifier circuit also incorporates special provisions for controlling the drive pulse width, as well as its phase lag [normally set at 90° relative to the detected signal to ensure resonance (French, 1970)].

Modeling

As mentioned earlier, the discharged particle size and its mass are respectively determined from the spring extension and resonant frequency. These are the two parameters required for obtaining the particle-size distribution data. In practice, however, as a consequence of the inevitable transverse bending of the spring during vibration, the actual particle size discharged is also dependent on the spring dynamic coil gap (also see later). This is in turn defined by its vibration profile or mode function. The following describes the development of a mathematical model for simulating the spring mode function as well as predicting the effect of spring tension and powder mass on the resonant frequency.

Vibration of the particle-size analyzer

Figure 2a shows a mechanical viscoelastic model adopted for describing the vibration characteristics of the particle-size analyzer. The system is divided into two main components comprising the "vibration generator" and the "particle size analyzer" (spring and supporting chamber) of mass, m. The symbols K and c represent the stiffness and damping coefficient (assumed to be of viscous type; Beards, 1995), respectively, of the vibration generator. On the other hand, the spring is assumed to be completely elastic.

The spring's vertical displacement at any point along its length is represented by y, whereas, y_2 is the corresponding displacement of the supporting chamber. For simple harmonic motion, the equivalent vertical displacement, y_1, of the input drive is given by

$$y_1 = A \sin \omega t, \tag{1}$$

where A and ω are the corresponding amplitude and angular frequency, respectively.

Figure 2b shows a force balance diagram for the particle-size analyzer. The corresponding equation of motion is

$$my_2'' = K(y_1 - y_2) + c(y_1' - y_2'), \tag{2}$$

where y_2'' is the acceleration, y_2' and y_1' are the velocities of particle-size analyzer and input drive, respectively. Substituting Eq. 1 and its derivative into Eq. 2 and rearranging, it follows that

$$my_2'' + cy_2' + Ky_2 = KA \sin(\omega t) + cA\omega \cos(\omega t). \tag{3}$$

Assuming

$$\alpha = \tan^{-1}(c\omega/K), \tag{4}$$

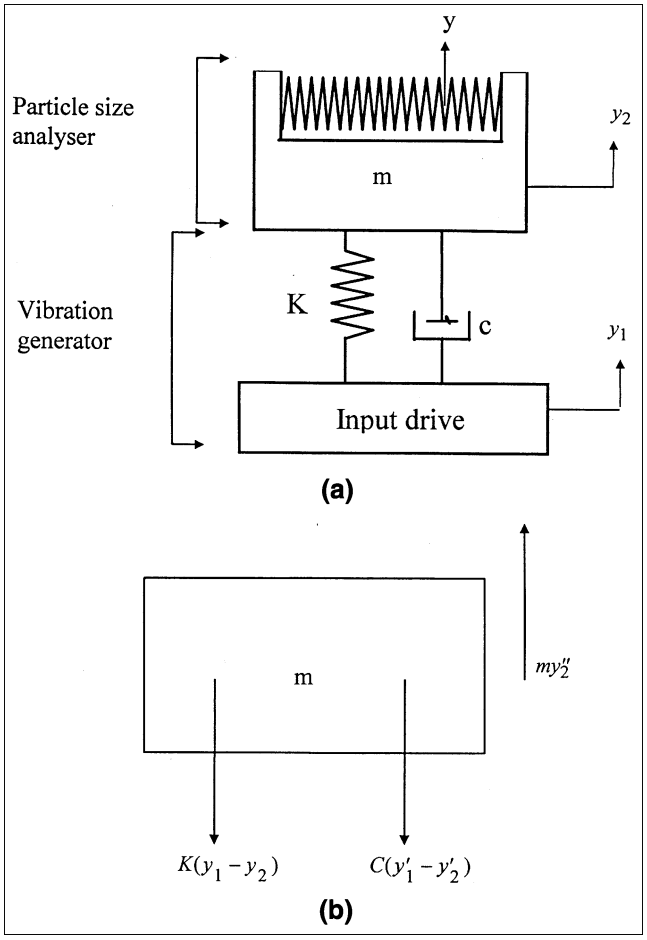

Figure 2. (a) Mechanical viscoelastic model showing vibration behavior of particle-size distribution analyzer; (b) force for particle-size distribution analyzer.

the differential equation of motion (Eq. 3) representing the absolute motion, y_2, can be written as

$$my_2'' + cy_2' + Ky_2 = A\left[K^2 + (c\omega)^2\right]^{0.5} \sin(\omega t + \alpha). \tag{5}$$

The auxiliary equation, where the righthand side of the preceding equation is taken as zero, gives the solution to the transient motion of vibration and is therefore not considered further. On the other hand, the steady-state solution can be obtained by using the method of undetermined coefficients (Goodman, 1980) such that

$$y_2 = B \sin(\omega t + \alpha - \phi). \tag{6}$$

Taking the first and second derivative of y_2 from Eq. 6 and substituting into Eq. 5, produces

$$B = \frac{A\sqrt{\left(K^2 + (c\omega)^2\right)}}{\sqrt{(K - m\omega^2)^2 + (c\omega)^2}}. \tag{7}$$

Here

$$\phi = \tan^{-1}\left(\frac{c\omega}{K - m\omega^2}\right). \tag{8}$$

For simplicity, we define $(\phi - \alpha) = \theta$, and hence Eq. 6 can be rewritten as

$$y_2 = B\sin(\omega t - \theta). \tag{9}$$

The ratio B/A is normally referred to as motion transmissibility (Beards, 1995) such that

$$\frac{B}{A} = \frac{\left[1 + (2\xi\omega/\omega_n)^2\right]^{0.5}}{\left[(1 - (\omega/\omega_n))^2 + (2\xi\omega/\omega_n)^2\right]^{0.5}}, \tag{10}$$

where ω_n and ξ are the natural frequency and damping ratio of the vibrating system, respectively, and are, in turn, given by

$$\omega_n = (K/m)^{0.5} \tag{11}$$

$$\xi = \frac{c}{2\sqrt{(Km)}}. \tag{12}$$

Equation 10 implies that when the drive frequency, ω, approaches the natural frequency, ω_n, of the system, a maximum value for the amplitude, B, will be expected.

Vibration of the spring

Unlike the simple one-dimensional motion of the discharge chamber, the motion of the spring is complex. Both spring ends are motionless relative to the chamber, while all other points along its length experience a vertical periodic oscillation. Assuming a Cartesian coordinate system, the vertical displacement, y, at any given point, P, at a distance, x, along the spring length is a function of time, t, so that

$$y = f(x,t) = Y + y_2, \tag{13}$$

where Y is the vertical displacement at point P relative to the chamber. Since no direct analysis describing the transverse vibration of a horizontally held helical spring is available, a theory (Hannah and Hillier, 1995) relating to a slender beam experiencing transverse vibration is adopted for this purpose. Conveniently, such an analysis takes into account the effect of spring moment of inertia and its tension. The slender-beam theory also assumes that the material is elastic, that the cross section is symmetrical about the plane of bending (otherwise the beam would twist as well as bend), and obeys Hooke's law. For a horizontal beam experiencing transverse vibration and subjected to an applied tensile force, T, the Euler equation is given by (Kelley, 1993)

$$EI_{\text{eq}}\frac{\partial^4 y}{\partial x^4} + T\frac{\partial^2 y}{\partial x^2} + \rho\frac{\partial^2 y}{\partial t^2} = 0, \tag{14}$$

where ρ is the mass per unit length of the beam, E is the Young's modulus, and I_{eq} is the spring equivalent moment of inertia. Differenting Eq. 9 with respect to time, t, rearranging and combining with Eqs. 13 and 14, produces

$$EI_{\text{eq}}\frac{\partial^4 Y}{\partial_x^4} + T\frac{\partial^2 Y}{\partial x^2} + \rho\frac{\partial^2 Y}{\partial t^2} + \rho\frac{\partial^2 y_2}{\partial t^2} = -\rho\omega^2 B\sin(\omega t - \theta). \tag{15}$$

Equation 15 is the fundamental equation representing the vibration characteristics of the spring, including its natural frequency, resonant frequency, and its corresponding vibration mode.

Spring shape function

Noting that Eq. 15 is linear, a harmonic response with the same angular frequency, ω, can be expected in the following form

$$Y(x,t) = f(x)\sin(\omega t - \theta), \tag{16}$$

where $f(x)$ is the spring mode function that is being sought. Differentiation of Eq. 16 followed by substitution into Eq. 15 produces

$$EI_{\text{eq}}\frac{d^4 f(x)}{dx^4} + T\frac{d^2 f(x)}{dx^2} - \rho\omega^2 f(x) = -\rho B\omega^2. \tag{17}$$

The complete solution of Eq. 17 by adopting a scientific guess method (Goodman, 1980) is given by

$$f(x) = c_1 e^{\alpha x} + c_2 e^{-\alpha x} + c_3\cos(\beta x) + c_4\sin(\beta x) + B, \tag{18}$$

where $c_1 - c_4$ are constants (see later). On the other hand, are α and β, the real and imaginary roots of Eq. 18's characteristic equation, respectively.

Now, as the two ends of the spring are clamped, the corresponding boundary conditions are as follows

$$f(x) = 0 \quad \text{and} \quad f(l) = 0 \tag{19}$$

$$df(x)/d(x)_{,x=0} = 0 \quad \text{and} \quad df(x)/d(x)_{,x=1} = 0, \tag{20}$$

where l is the length of the spring. Imposing the preceding boundary conditions on Eq. 18, a set of four equations leading to the calculation of the constants $c_1 - c_4$ can be found. These are given by

$$c_1 = \frac{\alpha(R_1Q_2 - R_2Q_1) - \beta(P_1R_2 + P_2R_1) + \alpha\beta(Q_1P_2 - P_1Q_2)}{2\alpha(Q_1P_2 + P_1Q_2)} \tag{21}$$

$$c_2 = \frac{\alpha(R_1Q_2 - R_2Q_1) - \beta(P_1R_2 - P_2R_1) + \alpha\beta(Q_1P_2 - P_1Q_2)}{2\alpha(Q_1P_2 + P_1Q_2)} \tag{22}$$

$$c_3 = \frac{R_1 Q_2 - R_2 Q_1}{Q_1 P_2 + P_1 Q_2} \tag{23}$$

$$c_4 = \frac{P_1 R_2 - P_2 R_1}{Q_1 P_2 + P_1 Q_2}. \tag{24}$$

The appropriate expressions for $P_{1,2}$ and $Q_{1,2}$ are given in the Appendix.

In accordance with Eqs. 21–24, the spring displacement profile, $f(x)$, approaches infinity if the following equation is satisfied

$$Q_1 P_2 + P_1 Q_2 = 0. \tag{25}$$

Substituting equations for P_{1-2} and Q_{1-2} given in the Appendix into Eq. 25 produces

$$\omega_r = \frac{T \sin(\alpha l)\cosh(\beta l)}{2(El_{eq}\rho)^{0.5}[\cos(\alpha l)\sinh(\beta l)] + 1}, \tag{26}$$

where ω_r is the resonant frequency of the spring.

Equations 18 and 26 can now be used respectively to generate the spring vibration profile (shape function) and predict its resonant frequency, as both equations are usefully expressed in terms of measurable parameters. The latter include spring tension, its design characteristics (moment of inertia, mass per unit length, stiffness, length, and Young's modulus) and also the vibration intensity. However, the prediction of the discharge particle size as a function of the spring mode shape also requires a knowledge of the spring dynamic coil gap.

Spring dynamic coil gap

Figure 3 provides an exaggerated representation of the dynamic and static spring profiles. The former is in the form of a half-wave, symmetrical about the midpoint along its length, as predicted from Eq. 19 and confirmed by experiment. For a given spring tension, the lower and upper bounds of the size of particles discharged from the spring are equal, respectively, to the static (d_s) and dynamic (d_d) coil gaps. The static coil gap is simply estimated by assuming uniform spring extension and dividing it by the number of coils. According to Figure 3, the angle θ is given by

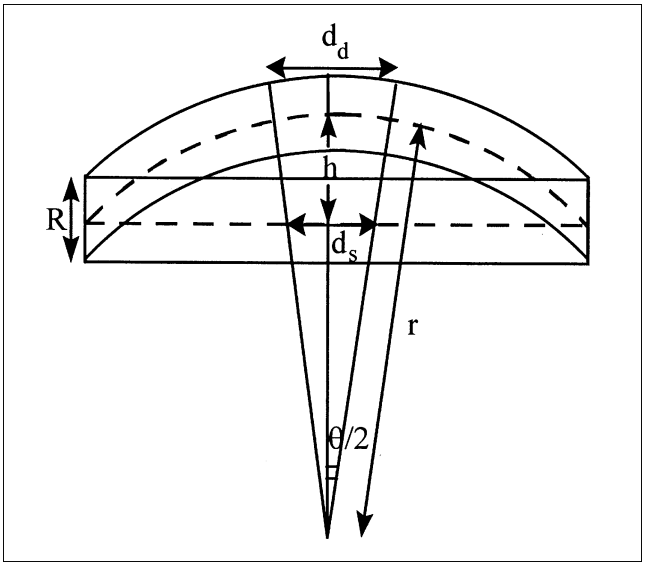

Figure 3. Dynamic and static spring vibration profiles.

$$\theta = 2\tan^{-1}[d_s/2(r-h)], \tag{27}$$

where h is the spring maximum deflection (obtained from the shape function; Eq. 19); r, on the other hand, is the radius of curvature of the spring mode measured from the spring main axis. It is given by the inverse of the second derivative of the shape function. Hence, from Eq. 19, we have

$$r = 1/f''(l) = 1/$$
$$\left[c_1\alpha^2 e^{\alpha l/2} + c_2\alpha^2 e^{-\alpha l/2} - c_3\beta^2\cos(\beta l/2) - c_4\beta^2\sin(\beta l/2)\right]. \tag{28}$$

Returning to Figure 3, the dynamic spring gap, d_d, can be expressed as

$$d_d = (r+R)\theta, \tag{29}$$

where R is the spring mean coil diameter. Substituting for θ given by Eq. 27 into the preceding equation produces

$$d_d = (r+R)\tan^{-1}\left[\frac{d_s}{2(r-h)}\right]. \tag{30}$$

Model Evaluation

Variation of resonant frequency with spring tension and sample mass

Figure 4 shows the variations of measured and predicted (Eq. 26) resonant frequencies with spring tension for various charge masses of glass Ballotini in the size range 1,000–1,200 μm. The maximum coil gap for all these tests is limited to about 800 μm, so that at no time are any of the particles discharged from the spring coils. The predicted data were generated based on the assumption that the sample mass is uniformly distributed along the spring length and that there is no relative motion between spring and the test particles during vibration. The former assumption is found to be generally valid as confirmed by visual inspection. The fact that the peak-to-peak amplitude of vibration of the spring is small (about 1 mm) partially fulfills the second assumption.

It is clear that there is a reasonably good agreement between theory and experiment.

Prediction of spring dynamic coil gap

The experimental dynamic coil gap was simply estimated by continuously extending the spring and noting the onset of

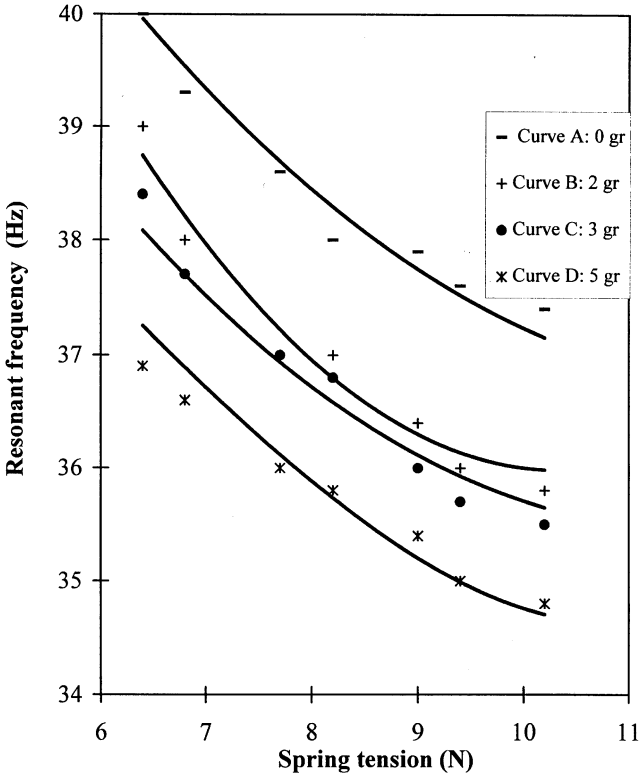

Figure 4. Predicted (solid lines) vs. experimental variation of spring resonant frequency with tension for various charge masses.

Curve A: 0 g; curve B: 2 g; curve C: 3 g; curve D: 5 g.

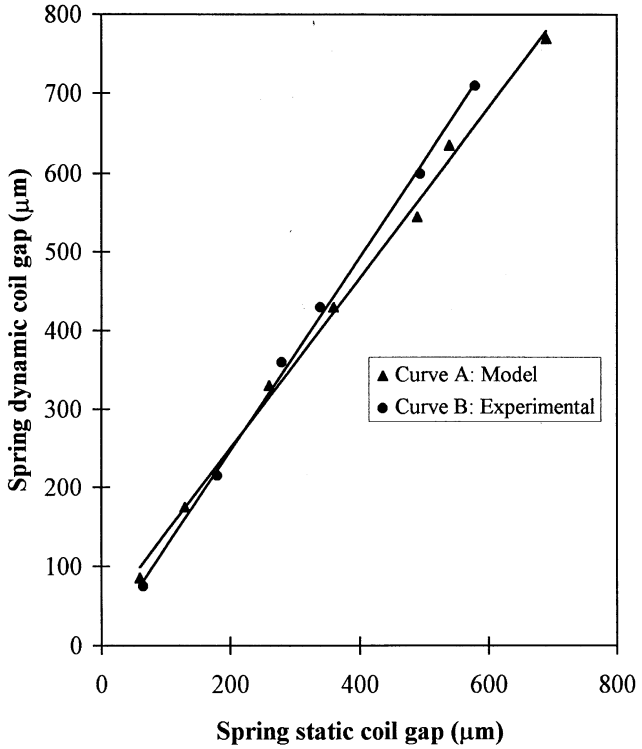

Figure 5. Variation of spring dynamic coil gap with static coil gap for various size 5-g charge samples of glass Ballotini vibrated at 37 Hz.

particulate discharge for a given sieve cut during resonance vibration. The dynamic coil gap was then equated to the upper size of the sieve cut at the corresponding spring linear extension.

Figure 5 shows the variation of the spring dynamic coil gap with static coil gap as predicted (Eq. 30, curve A) and from measurement (curve B) for various 5-g sieve cut sizes of glass Ballotini powder.

It is noted that there is a reasonably good agreement between theory and experiment. In addition, the fact that in all cases the spring dynamic coil gap is larger than the corresponding static coil gap underlines the importance of a knowledge of the spring vibration profile when performing size analysis.

The differences between the theoretical predictions and those from experiment (Figures 4 and 5) are due to a number of factors, the most important of which include the following:

1. The application of slender beam theory to a spring. This requires the fulfillment of a number of criteria relating to the deformation of the spring during transverse vibration (Hannah and Hillier, 1995).

2. The validity of the imposed spring shape function boundary conditions. In this study, we assume clamped ends, whereas in practice each spring end may experience a combination of clamped and hinged deformation.

3. Assumption of uniform static coil gap in response to spring extension.

Performance evaluation

Figures 6–9 show particle-size distribution data presented in the form of the variation of cumulative undersize percentage vs. particle size using the spring particle sizer and sieves for a range of powders with different density, shape, and flow characteristics. These include glass Ballotini (5 g, Figure 6), grit stone (8.5 g, Figure 7), sand (11 g, Figure 8), and sawdust (1.5 g, Figure 9). Each measurement is repeated twice in order to demonstrate the reproducibility in the data.

In the case of the spring particle sizer, each charge sample was extracted from a 1-kg batch using the cone and quarter procedure [British Standard 3406 (Part 1), 1986] in order to ensure statistical representation. Sieving was performed using approximately 1 kg samples in accordance with recommended practice (British Standard 1796 (Part 1), 1989).

Returning to the data, it is clear that in the case of glass Ballotini powder (Figure 6), the results obtained in conjunction with the two techniques are in good agreement. This is to be expected for spherical particles. The maximum deviation in size measurement between the two techniques is about 2.5%. In terms of reproducibility, the maximum discrepancy for the spring particle sizer is 3.5% (cf. 1% for sieves). On the other hand, the total analysis time using the current technique is about 3 min as compared to about 30 min using sieves for the same sample mass (5 g).

It is noteworthy that for different shaped particles (Figures 7–9), despite the very good reproducibility, the disagreement between the data obtained using the two techniques is more marked. For the same cumulative undersize percentage, the

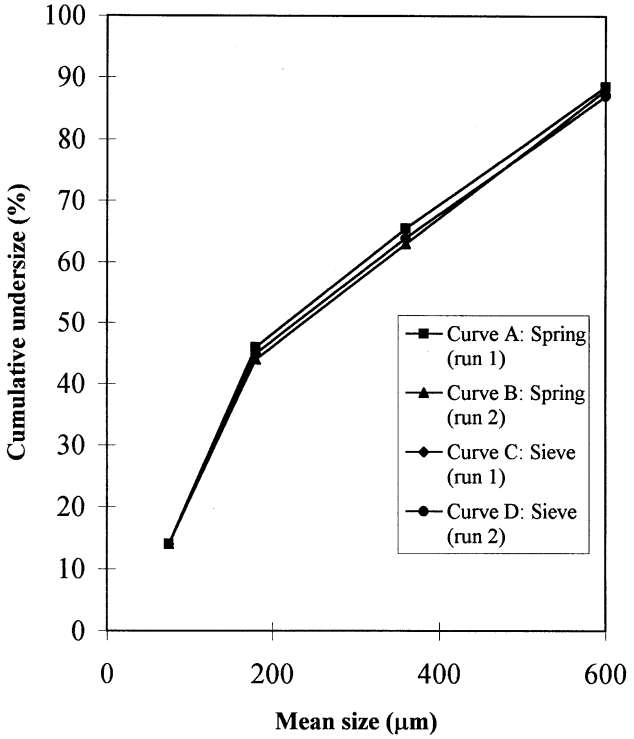

Figure 6. Variation of cumulative undersize percentage data with mean particle size for glass Ballotini.

Curve A: spring particle sizer (run 1); curve B: spring particle sizer (run 2); curve C: sieve data (run 1): curve D: sieve data (run 2).

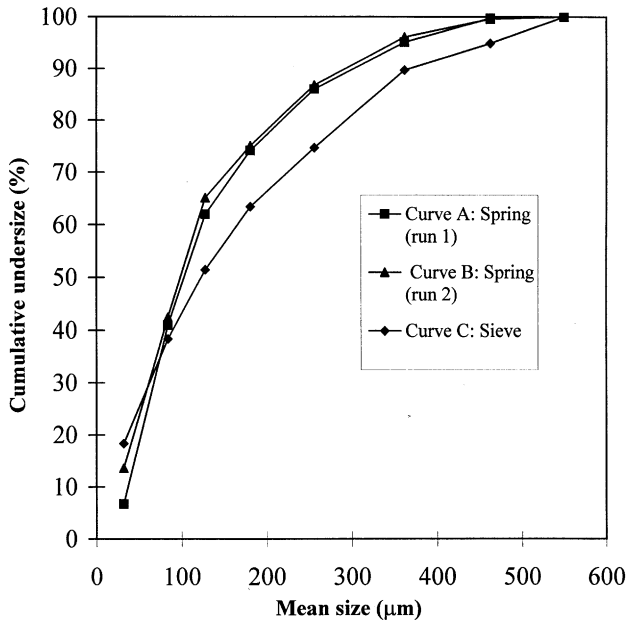

Figure 7. Variation of cumulative undersize percentage data with mean particle size for grit stone.

Curve A: spring particle sizer (run 1); curve B: spring particle sizer (run 2); curve C: sieve data.

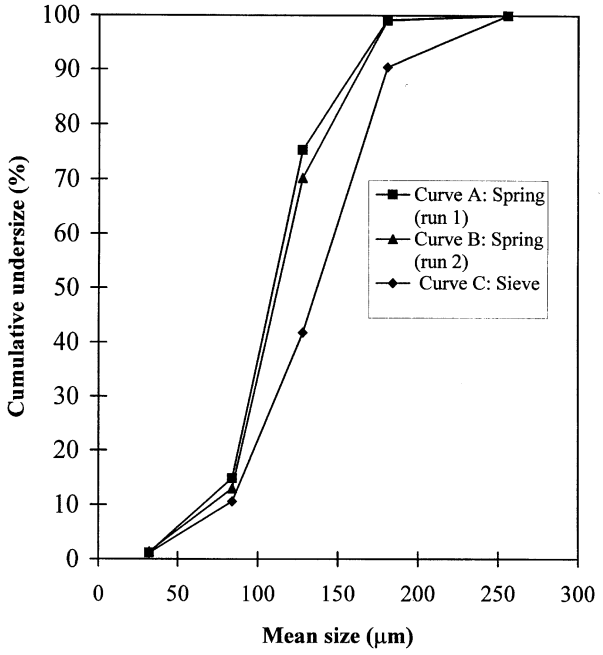

Figure 8. Variation of cumulative undersize percentage data with mean particle size for sand.

Curve A: Spring particle sizer (run 1); curve B: spring particle sizer (run 2; curve C: sieve data.

spring system consistently predicts a smaller particle size as compared to sieves. This is primarily a consequence of the different exit orientation of the test particles through the wire

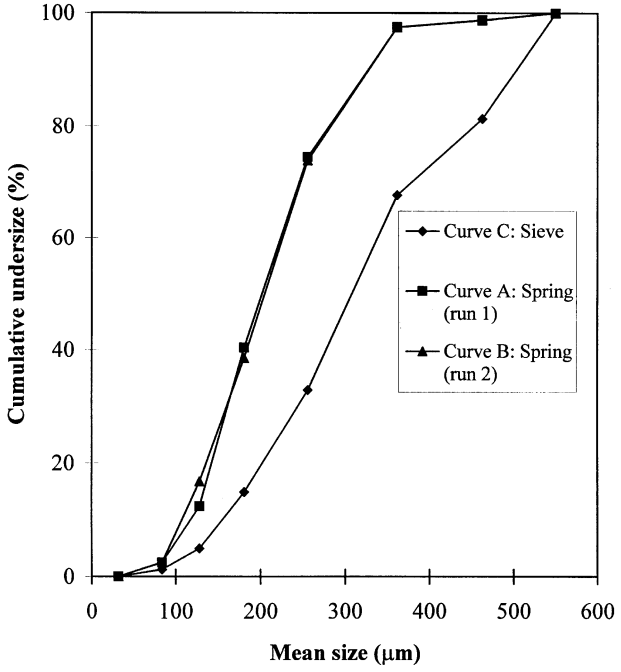

Figure 9. Variation of cumulative undersize percentage data with mean particle size for sawdust.

Curve A: Spring particle sizer (run 1); curve B: spring particle sizer (run 2); curve C: sieve data.

aperture for each method. Indeed, it is well established that particle sizing techniques based on different principles produce a different characteristic size (Mullin, 1993). British Standards (British Standard 3406: Part 3, 1996) provide various conversion factors for cross-correlation between some of the most common techniques. In this study, comparison between sieve data as compared to those from the spring produces modal and mean conversion factors of 1.3 and 1.5, respectively.

Conclusions

In this article we have described the basic design and modeling of the behavior of a novel technique for particle-size distribution analysis. The device is simple, robust, and does not require skilled operators. It is, in principle, capable of handling relatively large amounts of powder, thus overcoming sample representation problems, which is synonymous with a large majority of particle-sizing techniques available.

Although recent developments in laser particle-sizing technology allow the injection of relatively large amounts of the test particles in a laser beam, such instruments are extremely expensive. Also, they are not suitable for use in the aggressive environments typical of powder production plants.

As compared to sieves, the spring particle sizer is in principle capable of producing an infinite number of size fractions as opposed to the restricted numbers dictated by the number of sieve trays employed. A further problem associated with sieves is blinding (particles becoming trapped in the sieve apertures). In practice, this can result in significant "down time" resulting from having to clean the wire meshes. Also the cams that produce the shaking action wear, affecting reproducibility. Neither of these factors are a problem with the spring particle sizer. We find that the slight oscillatory variation of the spring coil aperture during vibration acts as a natural deblinding mechanism. Also, if any particles do eventually get trapped in between the spring coils, they are automatically dislodged as the spring is extended.

The possibility of automatically weighing the amount of sample *in situ* from the spring resonant frequency offers a significant reduction in testing time, thus making the technique particularly suited for process-control applications. In such circumstances, reproducibility is as important as absolute measurements, since operators are frequently interested in knowing whether the size distribution of a product is becoming coarser or finer. On-line applications can be served essentially by construction of a suitable sampler, allowing extraction, analysis, and recycling of test samples back into the process stream.

Apart from producing particle-size distribution data, the spring particle sizer also can be used, for example, as classifier, for separating an undersize powder from a given sample.

At present the system's resolution in size measurement is comparable to sieves. The mathematical model described in this study can be used as an invaluable tool for improving the system's performance. For example, a more accurate prediction of the discharged particle size for a given spring extension also requires a knowledge of the spring dynamic coil gap. The latter may be predicted from the simulated spring vibration profile. Additionally, the resolution in particle-size distribution measurement is directly governed by mass sensitivity, in turn dictated by the rate of change in resonant frequency with sample mass. Once again, the theoretical model presented here can be used to provide a rapid means for evaluating the effect of a number of design and operating parameters on mass sensitivity. These may, for example, include the spring coil diameter, wire thickness, mass, and the vibration intensity.

Acknowledgments

The technology described in this publication is subject to worldwide pattents.

Literature Cited

Allen, T., *Particle Size Measurement*, 5th ed., Vol. 1, Chapman & Hall, London (1997).

Beards, C. F., *Engineering Vibration Analysis with Application to Control Systems*, Arnold, New York (1995).

British Standard, "Methods for the Determination of Particle Size Powders," *Air Elutriation Methods*, BSI, 3406, Part 3 (1963).

British Standard, "British Standard Methods for Determination of Particle Size Distribution," *Guide to Powder Sampling*, BSI, 3406, Part 1 (1986).

British Standard, "Testing Sieving: Methods Using Test Sieves of Woven Wire Cloth and Perforated Metal Plate," BSI, 1796, Part 1 (1989).

Dockery, D. W., C. A. Pope, X. Wu, J. D. Spengler, J. H. Ware, M. E. Fay, B. G. Ferris, and F. E. Speizer, "An Association Between Air Pollution and Mortality in Six US Cities," *New Eng. J. Med.*, **329**, 1753 (1993).

French, A. P., *Vibration and Waves*, MIT Introductory Physics Series, Nelson, London (1970).

Geldart, D., "Powder Processing—The Overall View," *Principles of Powder Technology*, Wiley, London, (1990).

Goodman, A. W., *Analytical Geometry and the Calculus*, MacMillan, New York (1980).

Hanna, J., and M. J. Hillier, *Applied Mechanics*, Longmans, London (1995).

Kelley, S. G., *Fundamentals of Mechanical Vibrations*, McGraw-Hill, London (1993).

Mahgerefteh, H., and H.F. Al-Khoory, "Predictive Criteria for the Optimisation of a Vibrating Reed Transducer," *Trans. Inst. Meas. Control*, **13**, 48 (1991).

Mahgerefteh, H., H. F. Al-Khoory, and A. Khodaverdian, "Novel Thermogravimetric Analyser," *Thermochim. Acta.*, **237**, 175 (1994).

Mahgerefteh, H., and A. Khodaverdian, "Added Mass Effects in Two-Phased Solid/Liquid Media," *Trans. Inst. Chem. Eng. Res. Dev.*, **79**, 272 (1996).

Market Analysis and Perspective, Physical Property Measurements: Particle Characterization, Strategic Directions International Corporation, New York (1991).

Mullin, J. W., *Crystallisation*, 3rd ed., Butterworth-Heinemann, Oxford (1993).

Muly, E. C., and N. Frock, "Industrial Particle Size Measurement Using Light Scattering," *Opt. Eng.* **19**, 861 (1980).

Pope, C. A., M. J. Thun, N. M. Namboodiri, D. W. Dockery, J. S. Evans, F. E. Speizer, and C. W. Heath, "Particulate Air Pollution as a Predictor of Mortality in a Prospective Study of US Adults," *Amer. J. Respir. Crit. Care Med.*, **151**, 669 (1995).

Syvitski, P. P. M., *Principles, Methods and Applications of Particle Size Analysis*, Cambridge Univ. Press, Cambridge (1991).

Walters, S. R., K. Griffiths, and J. G. Ayres, "Temporal Association Between Hospital Admissions for Asthma in Birmingham and Ambient Levels of Sulphur Dioxide and Smoke," *Thorax*, **49**, 133 (1994).

Wen, C. Y., and Y. H. Yu, "A Generalized Method for Predicting the Minimum Fluidization Velocity," *AIChE J.*, **12**, 610 (1966).

Yates, J. G., P. N. Rowe, and D. J. Cheesman, "Gas Entry Effects in Fluidized Bed Reactors," *AIChE J.*, **30**(6), 890 (1984).

Appendix

Constants for Eqs. 21–24

$$P_1 = \alpha \cos(\beta l) + \beta \sin(\beta l) + \alpha e^{-\alpha l}$$

$$P_2 = \left[2\cos(\beta l) + e^{\alpha l} + e^{-\alpha l}\right]\alpha$$

$$R_1 = \alpha B e^{-\alpha l} - \beta\alpha$$

$$R_2 = \alpha\beta(2 + e^{\alpha l} - e^{-\alpha l})$$

$$= \left[(-T + \nabla)/2EI_{\text{eq}}\right]^{0.5}$$

$$Q_1 = \alpha \sin(\beta l) - \beta \cos(\beta l) - \beta e^{-\alpha l}$$

$$Q_2 = 2\alpha \sin(\beta l) - \beta e^{\alpha l} - \beta e^{-\alpha l}.$$

Definitions of α and β in Eq. 18

$$\alpha = \left[(-T + \nabla)/2EI_{\text{eq}}\right]^{0.5}$$

$$\beta = \left[(T + \nabla)/2EI_{\text{eq}}\right]^{0.5},$$

where ∇ is the determinant of the characteristic equation governing the vibration of a spring that is in turn defined as

$$\nabla = \left[T^2 - 4EI_{\text{eq}}\rho\bar{\omega}^2\right]^{-0.5},$$

where T and $\bar{\omega}$ are the tensile force and spring angular natural frequency, respectively.

Manuscript received Dec. 14, 1999, and revision received Aug. 11, 2000.